

FEDSM-ICNMM2010-0*

EXPERIMENTAL CHARACTERIZATION OF THE UNSTEADY FLOW OVER THE REAR SLANT OF AN AHMED BODY

Adrien Thacker

Institut PRISME

Écoulements et Système Aérodynamique

Université d'Orléans

8 rue Léonard de Vinci, 45074 Orléans FRANCE

Email: adrien.thacker@univ-orleans.fr

Sandrine Aubrun*

Annie Leroy

Philippe Devinant

Institut PRISME

Écoulements et Système Aérodynamique

Université d'Orléans

8 rue Léonard de Vinci, 45074 Orléans FRANCE

Email: sandrine.aubrun@univ-orleans.fr

ABSTRACT

This study presents results of an experimental analysis of the unsteady features of the flow around the rear part of an Ahmed body with a rear slant angle of 25° . This analysis focuses on the half elliptic separation bubble that develops on the rear slanted surface and brings new information, improving the understanding of the flow unsteadiness. Flow investigations are carried out using hot wire probe measurements for velocity fluctuations in the plane of symmetry above the rear slanted surface and five unsteady flush mounted pressure taps (Kulite transducers) simultaneously acquiring static pressure fluctuations along the middle line of the slanted surface. Spectral analysis and Proper Orthogonal Decomposition of the output signal show the emergence of a low frequency unsteadiness and high frequency activities which, in accordance with bibliography about separated and reattaching flow configurations, is related to a global flapping of the separated shear layer and a large scale vortices shedding. Characteristic frequencies of both instabilities is given and physical effects of the low frequency unsteadiness is related with the flapping motion of the separated shear layer.

NOMENCLATURE

- H Height of the Ahmed body.
- l Length of the rear window in the X,Y,Z reference axis.
- L Half width of the Ahmed model.
- l^* Length of the rear window in the X^*, Y^*, Z^* reference axis.
- U_0 Free stream velocity.
- Re Reynolds number based on the Ahmed model length.
- X_r Mean reattachment length in the X,Y,Z reference axis.
- X_r^* Mean reattachment length in the X^*, Y^*, Z^* reference axis.
- $E_{uu}(f)$ Power spectral density of the velocity fluctuations.
- Δf Spectrum frequency resolution.
- σ_u^2 Variance of velocity time series.
- $E_{pp}(f)$ Power spectral density of the wall static pressure fluctuations.
- σ_p^2 Variance of wall static pressure time series.
- f_{lf} Low frequency unsteadiness characteristic frequency.
- St_{lf} Low frequency unsteadiness Strouhal number based on f_{lf}, X_r^* and U_0 .
- f_{hf} Large scale vortices shedding frequency.
- St_{hf} Large scale vortices shedding Strouhal number based on f_{hf}, X_r^* and U_0 .
- $P(X^*, t_i)$ i^{th} instantaneous wall static pressure distribution along the middle line of the rear slanted surface.

* Address all correspondence to this author.

- $\langle P \rangle (X^*)$ Time averaged wall static pressure distribution along the middle line of the rear slanted surface.
- $p'(X^*, t_i)$ i^{th} instantaneous wall static pressure fluctuation profile along the middle line of the rear slanted surface.
- $a^{(n)}(t_i)$ n^{th} POD mode coefficient of the i_{th} instantaneous wall static pressure fluctuation profile.
- $\Phi^{(n)}(t_i)$ n^{th} POD mode basis function.
- n POD mode number.
- $P^{LOM}(X^*, t_i)$ Low order model of the i^{th} instantaneous wall static pressure distribution.
- $C_{p_{max}}^{LOM}(X^*)$ Maximum of the low order modeling instantaneous wall static pressure coefficient distribution.
- $C_{p_{min}}^{LOM}(X^*)$ Minimum of the low order modeling instantaneous wall static pressure coefficient distribution.

INTRODUCTION

Since pioneering experimental works of Onorato et al [1], Ahmed et al [2], and Lienhart and Becker [3], a large amount of information in relation with the complex three dimensional topology and aerodynamic features of road vehicles has been published using the Ahmed body [2] as a reference model and enabled drag reduction. Though, current knowledge of the flow around road vehicles no longer allows significant drag reduction and is often limited to time averaged information. Apart from some experimental [4, 5] or numerical [6–8] studies, physical mechanisms related to the unsteady process involved in the flow dynamics are rarely characterized, whereas they are of a significant interest especially for flow control applications.

The Ahmed body simplified car geometry constitutes a reference model. It is a parallelepiped with a slanted surface at the rear part reproducing the basic flow features at the rear part of vehicles. Ahmed et al [2] pointed out that the flow is mainly controlled by the slant angle (for a given Reynolds number) and suggested a classification of the averaged flow topologies. The case of a slant angle of 25° is particularly interesting. Indeed, this configuration presents a complex organization of the flow with a high drag level and is representative of the flow topology at the rear part of common fastback cars. In that case time-averaged flow presents a half elliptic separation region on the slanted surface with two strong longitudinal vortices growing up at each side edge. In addition, at the rear base the mean flow shows strong toric structures (Fig. 1).

From a unsteady point of view the toric structures are intermittently shed and convected away of the model [4] while the longitudinal vortices are considered to be strongly stable [7]. Unsteadiness in the separation bubble that develops on the slanted surface has rarely been investigated. Numerical study of Krajnovic and Davidson [7] and Minguéz et al [8] using Large Eddy Simulation provided some new information about the instantaneous flow topology around the Ahmed body. Using Q criterion visualization of the instantaneous flow fields, these authors

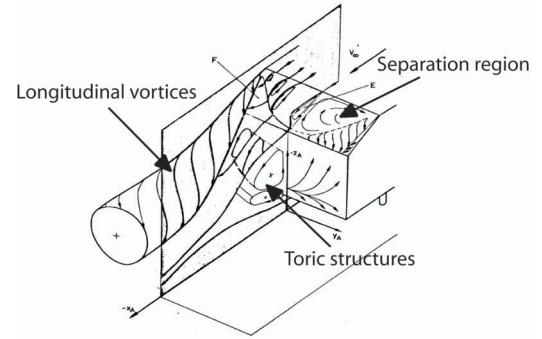


FIGURE 1. FLOW TOPOLOGY AT THE REAR PART OF THE AHMED BODY (AHMED ET AL [2])

pointed out hairpin-like vortices emission induced by the separated shear layer. In the same manner, another Large Eddy Simulation of the flow around the Ahmed body performed by Hinterberger et al [9] related that two typical instantaneous velocity fields could be found in the median plane of the slanted surface. In the first one the flow tends to reattach on the surface, and in the second one the flow is completely separated. A previous experimental analysis, deduced from the PIV measurements presented in this paper by conditionnally averaged instantaneous velocity fields of the separation bubble using the first Proper Orthogonal Decomposition mode coefficients, could confirm this two typical features [10]. This tendency suggests a flapping motion of the separated shear layer. However, these last authors do not clearly provide a complete description of these mechanisms as no experimental data are still available concerning these phenomena for the Ahmed body flow configuration. Moreover unsteady analyses of these mechanisms are still poor as no accurate spectral analyses has been provided.

In a more general context, unsteady mechanisms of separated and reattaching flow configurations have been widely characterized and represent a significant interest in this present application. Pioneer experimental works of Cherry et al [11] and Kiya and Sasaki [12, 13] dealing with unsteady measurements in a separation bubble formed at the leading edge of a blunt flat plate have shown that the unsteady flow is mainly governed by two agents : the motion of large scale vortices shed downstream the reattaching zone and the low-frequency unsteadiness associated with a flapping motion of the separated shear layer. These unsteady mechanisms are still reported in more recent literature [14–17] and present strong similarities with observations of Krajnovic and Davidson, Minguéz et al and Hinterberger et al [7–9].

For these reasons, this present paper deals with a preliminary experimental investigation of the unsteadiness related to the turbulent separation zone that develops on the slanted surface

of the Ahmed body. The aim of this investigation is to provide accurate frequency analysis and new experimental information to complete the characterization of the complex topology of the flow around the Ahmed body going by the observations of Krajinovic and Davidson, Minguéz et al and Hinterberger et al [7–9] and the unsteady process described by Cherry et al [11] and Kiya and Sasaki [12, 13]. The flow investigation is carried out using a hot wire probe in the plane of symmetry above the rear slanted surface and five unsteady flush mounted pressure taps (Kulites) measuring the wall static pressure along the middle line of the slanted surface.

After presenting the mean topology of the separation bubble that develops on the rear slanted surface by means of PIV measurements, spectral analyses of velocity and wall pressure fluctuations will be performed. The characteristic frequencies related to the flow dynamics in this region will be then extracted. At last Proper Orthogonal Decomposition (POD) method will be applied to the instantaneous wall pressure profiles to exhibit the unsteady behaviour of the separation bubble.

EXPERIMENTAL SET UP

Test Model and Wind Tunnel

The model used for this study is the Ahmed body reference model [2] with a 25° rear slant angle. Main dimensions of the model are given on Fig. 2. Tests were run in the wind tunnel "Lucien Malavard" at the PRISME institute of the University of Orléans, FRANCE. The square test section is 2m x 2m and 5m long. The Ahmed body was fixed above a streamlined plate board (2m wide and 3m long) placed 480 mm above the wind tunnel ground. The leading edge of the plate board is elliptic and an inclinable trailing edge flap avoids any longitudinal pressure gradient. All tests were run with a freestream velocity of $U_0 = 30\text{m/s}$ corresponding to a model length based Reynolds number of 2.2 millions. For this freestream velocity, the boundary layer that develops on the plate board was 20mm thick with a distance between the plate board and the model of 50mm.

Particle Image Velocimetry System

Spatial characterization of the flow on the rear slanted surface was carried out using PIV. It consists of a double pulsed Nd:Yag laser emitting pulses of 200mJ. The laser light sheet was set parallel to the streamwise direction at the median plan $Y=0$. Images were acquired with a TSI Power View Plus 2048 x 2048 pixels camera fitted with 105mm lens. The camera was located in the direction normal to the laser sheet and was inclined 25°. Images are then set in the $(X^*, Y^* = 0, Z^*)$ reference axis (see Fig. 3). The image size is 219mm x 219mm and therefore images cover the whole separation region. The seeding consisted of submicrosized olive oil droplets sprayed by a PIVTEC seeding system. For this configuration 500 image pairs were recorded

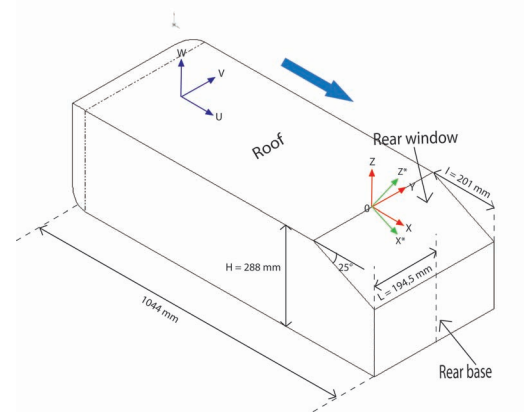


FIGURE 2. BASIC DIMENSION AND REFERENCE AXIS OF THE AHMED MODEL

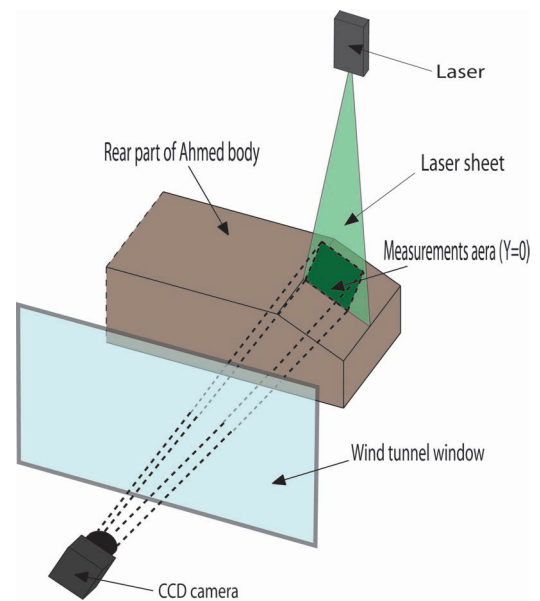


FIGURE 3. PIV SYSTEM CONFIGURATION

to ensure good statistics.

Post processing were carried out using 255 x 255 interrogation windows of 16 x 16 pixels with an overlap rate of 50%. The space resolution is then 0.9mm.

Hotwire Anemometer and Wall Pressure Measurements Set Up

In order to investigate the unsteadiness within and in the surrounding of the separating/reattaching flow region of the rear slanted surface, time series of the velocity and wall pressure fluctuations were recorded.

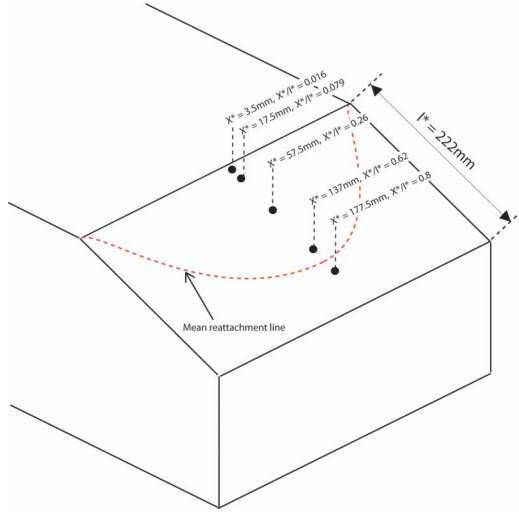


FIGURE 4. KULITES POSITIONS

Velocity magnitude fluctuations were measured by using a DANTEC miniature 1D 55P11 hot wire probe connected to the DANTEC streamline system. Time series were recorded at two different locations in the median plane $Y = 0$: At $X = 50\text{mm}$ ($X/l = 0.25$), $Z = 0$, close to the flow separation, and at $X = 150\text{mm}$ ($X/l = 0.75$), $Z = -25\text{mm}$ ($Z/H = -0.09$), close to the reattaching zone (see Fig. 5). The sampling frequency was 2kHz and the sampling time was 61 minutes at each location allowing a sufficient resolution of high and low frequencies.

Wall static pressure fluctuations were measured along the center line of the slanted surface by using five unsteady flush mounted pressure taps (locations are given in Fig. 4): KULITE miniature XCQ062 pressure transducers with a sensing diameter of 1.7mm simultaneously acquiring signal using National Instruments A/D boards. The sampling frequency was 20kHz and the sampling time was 7 min. Anti-aliasing filters are used with a cut-off frequency of 10kHz.

RESULTS AND ANALYSIS

Mean Flow Topology

Contours and streamlines of the mean velocity field in the median plane of the slanted surface are presented in Fig. 5. As expected, results show the development of a recirculating zone due to a flow separation from the sharp edge between the roof and the slanted surface and a flow reattachment farther on the rear window. From a three-dimensional point of view this recirculating zone forms a half elliptical separation region as described by Ahmed et al [2]. The mean reattachment point is located at $X_r/l = 0.75$ which corresponds to $X_r^*/l^* = 0.73$ in the slanted surface reference axis (where $l^* = 222\text{mm}$ is the rear window length).

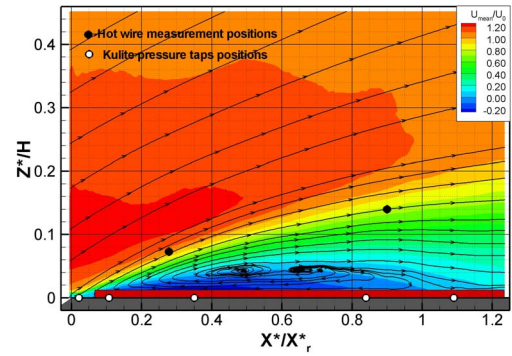


FIGURE 5. CONTOURS AND STREAMLINES OF THE MEAN VELOCITY FIELD OVER THE SLANTED SURFACE

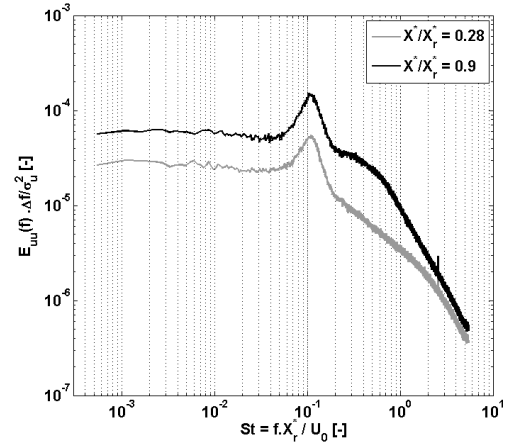


FIGURE 6. VELOCITY SPECTRUM

Unsteady Analysis

Wall Pressure and Velocity Spectrum. Dimensionless power spectral densities $E_{uu}(f) \cdot \Delta f / \sigma_u^2$ of the measured velocity time series are presented in Fig. 6. Results clearly indicate the emergence of a low frequency spectral activity. For both measurement locations, this is characterized by a dominant frequency of $f_{lf} = 20\text{Hz}$ that corresponds to a Strouhal number St_{lf} (based on the mean reattachment length X_r^* and the freestream velocity U_0) of 0.11. This Strouhal number is consistent with the observation of Cherry et al [11] and Kiya and Sasaki [12, 13] for a separation bubble formed at the leading edge of a blunt flat plate who found a Strouhal number of 0.12 associated with the low-frequency unsteadiness.

Dimensionless power spectral densities of the measured wall pressure time series $E_{pp}(f) \cdot \Delta f / \sigma_p^2$ are presented in Fig. 7. As observed with the velocity spectra the low frequency spectral activity is well defined with a dominant frequency of $St_{lf} = 0.11$.

While moving downstream this signature is encountered near the separation zone ($X^*/X_r^* = 0.02$ and 0.11) and weakless in the mean reattachment zone ($X^*/X_r^* = 0.84$) and totally disappears within the separation bubble ($X^*/X_r^* = 0.35$) and downstream of $X^*/X_r^* = 1.1$. These observations are also reported by Cherry et al [11].

These results are thus consistent with the low frequency unsteadiness phenomena observed for separated and reattaching flow configurations. In accordance with the literature [9, 13] this spectral activity seems to be associated with a flapping motion of the separated shear layer.

For all locations the wall pressure spectra also indicate an activity at higher frequencies characterized by a spectral bump which is shifted toward the low frequency domain while moving downstream. In the separation zone this high frequency bump decreases from $f \approx 1kHz$ at $X^*/X_r^* = 0.02$ to $f \approx 500Hz$ at $X^*/X_r^* = 0.11$ and attains a constant frequency domain of $f \approx 100Hz$ from $X^*/X_r^* = 0.35$ up to $X^*/X_r^* = 1.1$.

From the study of Cherry et al [11] and Kiya and Sasaki [12, 13] this observation is associated with the large scale vortices emission. Thus an amalgamation process of small scale vortices resulting from Kelvin-Helmholtz instability forms large scale structures inducing a decrease of the frequency bump toward the low frequency domain. These large scale structures are finally shed downstream of the reattaching zone with a constant characteristic frequency [11, 12, 14, 17]. This mechanism is also supported by the Large Eddy Simulation of the flow around the Ahmed body performed by Krajnovic and Davidson and Minguez et al [7, 8] who observed hairpin like vortices emission. However these last authors do not provide precise characteristic frequencies of this phenomena.

Wall pressure spectra presented in this investigation are thus consistent with the bibliography concerning a large scale vortices emission. Indeed a constant range of frequency is reached from $X^*/X_r^* = 0.35$, the assumption is made that it corresponds to the large scale vortice frequency. This one is estimated to be $f_{hf} \approx 100Hz$ that corresponds to the reattachment length based strouhal number of $St_{hf} = 0.54$. This is in good agreement with previous studies of this typical separation bubble [11, 12, 14].

Proper Orthogonal Decomposition of Wall Pressure Measurements As described by the wall pressure and the velocity spectra the turbulent separation bubble over the rear slanted surface of the Ahmed body is characterized by two dominant processes : a low frequency unsteadiness with a dominant Strouhal number of $St_{lf} = 0.11$ and higher frequency activities decreasing down to a Strouhal number of $St_{hf} = 0.54$.

Thus, to complete this unsteady characterization, this part deals with the application of the Proper Orthogonal Decomposition (POD) [18] to the instantaneous wall pressure profiles along the turbulent separation bubble. The main issue is that instantane-

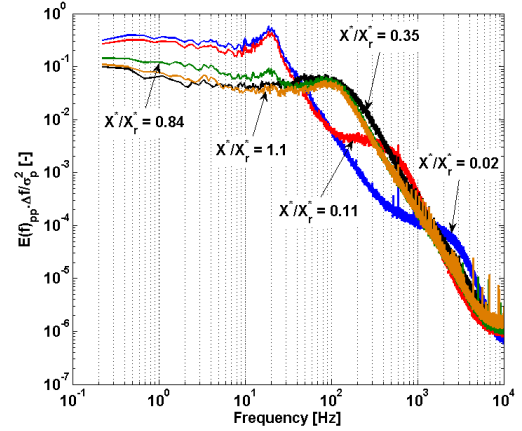


FIGURE 7. WALL-PRESSURE SPECTRUM

ous wall pressure profiles contain a great amount of information especially related to the turbulent motion and so significant characteristics of the flow are easily lost or screened. For this reason POD analysis represents an interesting way to get filtered information. The aim of this analysis is to distinguish the physical contribution of each dominant process on the wall pressure profile to confirm the assumption of a global flapping and vortex shedding mechanisms.

Basically, POD consists in expressing each instantaneous wall pressure profile $P(X^*, t_i)$ at a time t_i as Eqn. (1) :

$$P(X^*, t_i) = \langle P \rangle (X^*) + p'(X^*, t_i) = \langle P \rangle (X^*) + \sum_{n=1}^{Nt} a^{(n)}(t_i) \Phi^{(n)}(X^*) \quad (1)$$

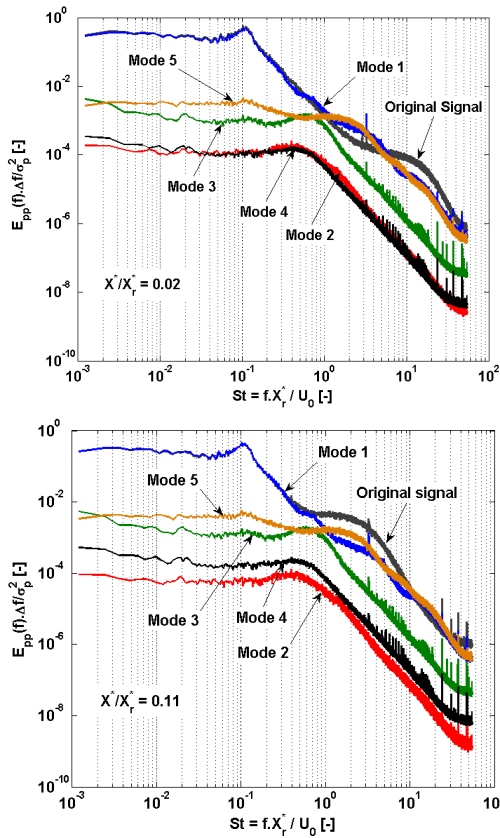
where $\langle P \rangle (X^*)$ and $p'(X^*, t_i)$ denote the time averaged and the fluctuating part of the wall pressure distribution respectively, $\Phi^{(n)}(X^*)$ is the n^{th} POD basis function. $a^{(n)}(t_i)$ is the n^{th} POD mode coefficient related to the i^{th} instantaneous wall pressure profile, and $n = 1..Nt$ is the POD mode number and Nt is the total number of POD modes. Using classical POD, the number Nt is equal to 5 (number of measurement locations). For more details about POD applications the reader is referred to [19].

The contribution of the five POD modes to the mean turbulent kinetic energy is presented in Table 1. Results show that the contribution of the energy content decreases from 44.5% for the first POD mode to 3.8% for the fifth mode. The three first POD modes represent approximately 84% of the energy contents.

The determination of each POD mode basis function $\Phi^{(n)}(X^*)$ and coefficient $a^{(n)}(t_i)$ is used to reconstruct time series of the wall pressure fluctuations at each measurement locations. As a result, for each measurement location, the wall pressure spectra can be reconstructed for each POD mode independently. Thus by comparing the original signal with each five mode reconstructions, the contribution of each POD mode to the low and

TABLE 1. CONTRIBUTION TO THE TURBULENT KINETIC ENERGY OF THE FIVE POD MODE.

Mode number	Contribution to the turbulent kinetic energy [%]
1	44.5
2	24.4
3	15.3
4	11.9
5	3.8



high frequency unsteadiness can be extracted.

The wall pressure spectra of the real signal and POD reconstructions for every measurement locations are presented in Fig. 8. Near the mean separation zone ($X^*/X_r^* = 0.02$ and 0.11) results indicate that the first POD mode spectrum coincides with the real signal in the low frequency domain. The low frequency

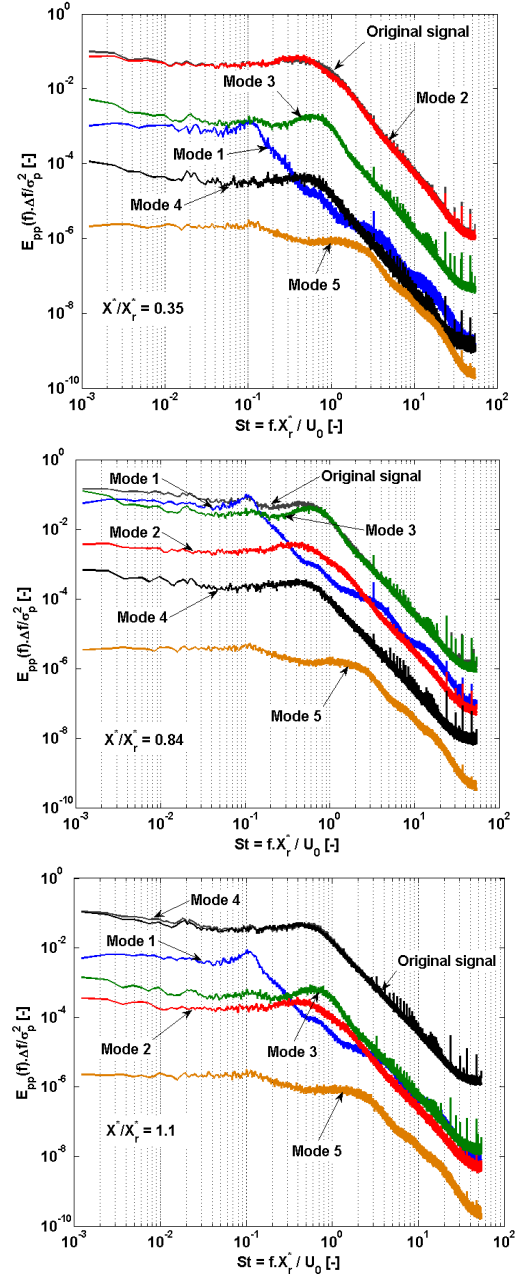


FIGURE 8. POD WALL-PRESSURE SPECTRA

unsteadiness ($St_{lf} = 0.11$), mostly observed near the separation point, is then well represented by the first POD mode.

Within the separation bubble ($X^*/X_r^* = 0.35$), the first POD mode is no more predominant and the second mode mostly becomes representative. In this case the low frequency unsteadiness is totally absent and wall pressure fluctuations are more specifically affected by the higher frequency activities ($St_{hf} \approx 0.54$) notably reproduced by the second POD mode.

Near the mean reattachment zone ($X^*/X_r^* = 0.84$), the wall pressure spectrum shows both low frequency unsteadiness and high frequency activities. In this case wall pressure fluctuations are dominated by the first and third POD modes. The predominance of the first mode is found again in the low frequency domain and the low frequency unsteadiness is reproduced. In the high frequency domain the first mode is no more representative and the third mode is more adapted to reproduce the high frequency activities.

Finally, after the mean reattachment zone ($X^*/X_r^* = 1.1$), the low frequency unsteadiness disappears as the first POD mode becomes negligible and the fourth mode is clearly representative.

In conclusion of these results, it appears from the POD decomposition of the wall pressure spectra, that the first and the most energetic POD mode is associated with the low frequency unsteadiness while the others are clearly linked with the higher frequency activities. The present POD analysis, by automatically sorting information in the energetic decreasing order, allows a decomposition of the wall pressure fluctuations in respect with the two unsteady mechanisms.

The next analysis suggests a decomposition of the instantaneous wall pressure profiles by separating the low frequency unsteadiness from the wall pressure time series. The aim of this decomposition is notably to establish a link between the low frequency unsteadiness and the global flapping of the shear layer as suggested in the literature. This can be obtained with a low order model including the mean pressure profile and the first POD mode modelisation of pressure fluctuations. Each low order model of instantaneous pressure profile $P^{LOM}(X^*, t_i)$ is then computed using Eqn. (2) :

$$P^{LOM}(X^*, t_i) = \langle P \rangle (X^*) + a^{(1)}(t_i) \Phi^{(1)}(X^*) \quad (2)$$

where $a^{(1)}(t_i)$ is the first POD mode coefficient of the i^{th} instantaneous wall pressure profile. It quantifies the weight of the first POD mode in the i^{th} instantaneous wall pressure profile. Consequently the extremum of the first mode coefficients $a_{min}^{(1)}$ and $a_{max}^{(1)}$ represent the minimum and the maximum values of wall pressure fluctuations induced by the first POD mode respectively. Thus the low order model of the instantaneous wall pressure profiles corresponding to these coefficients represent the extremum configuration of instantaneous wall pressure profiles in respect with the first POD mode.

The difference between the extremum low order modeling of the wall pressure coefficient profiles (defined by Eqn. (3)) and the mean wall pressure coefficient profile is plotted on Fig. 9. Results show that the minimum low order modeling instantaneous profile $C_{P_{min}}^{LOM}(X^*)$ is greater than the mean wall pressure coefficient in the first part of the separation bubble ($X^*/X_r^* < 0.4$) and lower in the second part ($X^*/X_r^* > 0.4$). On the contrary the maximum

low order modeling instantaneous profile $C_{P_{max}}^{LOM}(X^*)$ is lower in the first part and more important in the second part.

$$C_{P_{max}}^{LOM}(X^*) = \frac{P_{ref} - P_{max}^{LOM}(X^*)}{\frac{1}{2} \rho U_0^2}$$

$$C_{P_{min}}^{LOM}(X^*) = \frac{P_{ref} - P_{min}^{LOM}(X^*)}{\frac{1}{2} \rho U_0^2}$$

where

$$P_{max}^{LOM}(X^*) = \langle P \rangle (X^*) + a_{max}^{(1)} \Phi^{(1)}(X^*) \quad (3)$$

$$P_{min}^{LOM}(X^*) = \langle P \rangle (X^*) + a_{min}^{(1)} \Phi^{(1)}(X^*)$$

The point $X^*/X_r^* = 0.4$ here corresponds to the location where $C_{P_{min}}^{LOM}(X^*)$ and $C_{P_{max}}^{LOM}(X^*)$ both match the mean wall pressure coefficient. It corresponds to the position X^* where the basis function $\Phi^{(1)}(X^*)$ is equal to zero. In other words this position is not affected by pressure fluctuations induced by the first POD mode.

From a physical point of view this mechanism is consistent with observations of Kiya and Sasaki [13] explaining the influence of the global flapping of the shear layer on the wall pressure distribution. According to these authors, when the shear layer moves from its mean position towards the surface, the longitudinal velocity at the edge increases because of an increased curvature of the shear layer near the separation zone. The wall pressure then becomes lower than the mean wall pressure. This "shrinkage" mechanism of the separation bubble is then characterized by negative pressure fluctuations near the separation zone. Inversely, when the shear layer moves outwards ("enlargement" mechanism) from its mean position, a decrease in the curvature of the shear layer leads to positive pressure fluctuations near the separation zone. These authors also indicate that the pressure fluctuations near the separation zone is 180° out of phase with the pressure fluctuations near the reattachment zone. That is to say the "shrinkage" mechanism is characterized by positive pressure fluctuations near the reattachment zone while the "enlargement" mechanism is characterized by negative pressure fluctuations at this same zone.

This "shrinkage/enlargement" mechanism presents a strong similarity with the first mode low order model. Thus $C_{P_{max}}^{LOM}(X^*)$ would correspond to the shrunk state of the separation bubble and $C_{P_{min}}^{LOM}(X^*)$ to the enlarged state. As a result it clearly appears that the low frequency unsteadiness observed in the wall pressure spectra, and reproduced by the first POD mode, is closely related with a flapping motion of the shear layer.

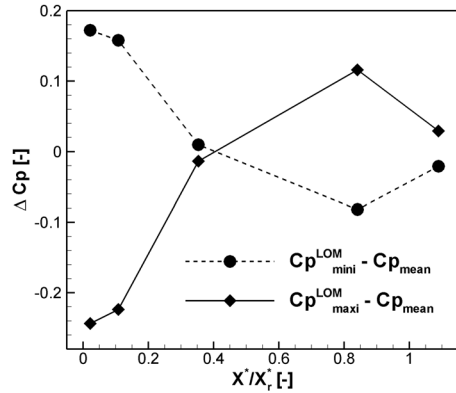


FIGURE 9. LOW ORDER MODELLING

CONCLUSIONS

The unsteady mechanisms of the separation bubble that develops on the rear slanted surface of the Ahmed model with a slant angle of 25° has been investigated using hot wire anemometer and Kulite pressure transducers. This investigation was based on a preliminary spectral analysis of the velocity and the wall static pressure fluctuations and on a Proper Orthogonal Decomposition of fluctuating wall pressure. The aim of this study was then to extract the characteristic frequencies related to the flow dynamics and their physical contribution to the unsteady behaviour of the separation bubble.

At last spectral analysis show the emergence of a low frequency unsteadiness with a Strouhal number of $St_{lf} = 0.11$ and high frequency activity with a dominant spectral bump of $St_{hf} = 0.54$. In accordance with the literature concerning unsteady mechanisms of separated and reattaching flow, these two characteristic frequencies are respectively related to a global flapping motion of the separated shear layer and a large scale vortices emission.

The application of the Proper Orthogonal Decomposition to the fluctuating wall static pressure has shown that the first and most energetic POD mode is mostly representative of the low frequency unsteadiness in the wall pressure fluctuation spectra while the large scale shedding is represented by the higher order POD mode. Finally low order modeling of instantaneous wall pressure profiles including only the first POD mode has shown that the physical effect of the low frequency unsteadiness is related to the mechanism of the flapping motion of the separated shear layer in accordance with the bibliography.

All of these results are consistent with previous numerical works concerning flow around the rear part of the Ahmed body [7–9] but bring some new unanswered questions. First of all the physical mechanism responsible of the global flapping is still unknown whereas it represents a significant interest in sight of flow control applications. Secondly, this study only focuses on

the median plane of the rear slanted surface and do not take into account the three dimensional aspects of both unsteady mechanisms.

This present study completes a previous characterization of the instantaneous velocity fields from the PIV measurements presented in this paper [10]. The use of the first POD mode coefficients to conditionally averaged instantaneous velocity fields could confirm that the separation bubble presents a enlarged and a shrunk state that is related to the flapping motion.

As a perspective to this study, next works will focus more particularly on the large scale vortices characterization through cross spectrum and cross correlation analyses.

REFERENCES

- [1] Onorato, M., Costelli, A., and Garonne, A., 1984. "Measurement through wake analysis". *SAE International Congress Exposition*, **SAE SP-569**, pp. 85–93.
- [2] Ahmed, S., Ramm, R., and Falting, G., 1984. "Some salient features of the time averaged ground vehicle wake". *SAE Technical Paper Series*, **840300**.
- [3] Lienhart, H., and Becker, S., 2003. "Flow and turbulence structure in the wake of a car model". *SAE World Congress*.
- [4] Vio, G., Watkins, S., Mousley, P., Wattmuff, J., and Prasad, S., 2005. "Flow structures in the near-wake of the ahmed model". *Journal of Fluids and Structures*, **20**, pp. 673–695.
- [5] Sims-Williams, D., and Duncan, B., 2003. "The ahmed model unsteady wake : Experimental and computational analyses". *SAE World Congress*.
- [6] Horward, R., and Pourquie, M., 2002. "Large eddy simulation of an ahmed reference model". *Journal of Turbulence*, **3**.
- [7] Krajnovic, S., and Davidson, L., 2005. "Flow around a simplified car". *Journal of Fluids Engineering*, **127**, pp. 907–928.
- [8] Minguez, M., Pasquetti, R., and Serre, E., 2008. "High-order large eddy simulation of flow over the ahmed body car model". *Physics of Fluids*, **20**, pp. 1–17.
- [9] Hinterberger, C., Garcia-Villabla, M., and Rodi, W., 2003. "Large eddy simulation of flow around the ahmed body". In *The Aerodynamics of Heavy Vehicles : Trucks, Buses and Trains*, R. McCallen, F. Browand, and J. Ross, eds., Vol. 20 of *Lecture Notes in Applied and Computational Mechanics*. pp. 77–89.
- [10] Thacker, A., Aubrun, S., Leroy, A., and Devinant, P., June 2010. "Unsteady analyses of the flow separation on the rear window of a simplified ground vehicle model". *28th AIAA Applied Aerodynamics Conference (paper accepted for presentation)*.
- [11] Cherry, N., R.Hillier, and Latour, M., 1984. "Unsteady

- measurements in a separated and reattaching flow”. *Journal of Fluid Mechanics*, **144**, pp. 13–46.
- [12] Kiya, M., and Sasaki, K., 1983. “Structure of a turbulent separation bubble”. *Journal of Fluid Mechanics*, **137**, pp. 83–113.
- [13] Kiya, M., and Sasaki, K., 1985. “Structure of large-scale vortices and unsteady reverse flow in the reattaching zone of a turbulent separation bubble”. *Journal of Fluid Mechanics*, **154**, pp. 463–491.
- [14] Hudy, L., Naguib, A., and Humphreys, W., 2003. “Wall-pressure-array measurements beneath a separating/reattaching flow region”. *Physics of Fluids*, **15**(3), pp. 706–717.
- [15] Chun, S., Liu, Y., and Sung, H., 2004. “Wall pressure fluctuations of a turbulent separated and reattaching flow affected by an unsteady wake”. *Experiments in Fluids*, **37**, pp. 531–546.
- [16] Largeau, J., and Moriniere, V., 2007. “Wall pressure fluctuations and topology in separated flows over a forward-facing step”. *Experiments in Fluids*, **42**, pp. 21–40.
- [17] Lee, I., and Sung, H., 2001. “Characteristics of wall pressure fluctuations in separated and reattaching flows over a backward-facing step : Part i. time mean statistics and cross-spectral analyses”. *Experiments in Fluids*, **30**, pp. 262–272.
- [18] Lumley, J., 1967. “The structure of inhomogeneous turbulence”. In *Atmospheric Turbulence and Wave Propagation*, A. Yaglom and V. Tatarski, eds. pp. 166–178.
- [19] Cordier, L., 2008. “Proper orthogonal decomposition : an overview”. In *Post-Processing of Numerical and Experimental Data*, Von Karmann Institute Lecture Series.